Drop-Size Distributions and Spatial Distributions in an Annular Centrifugal Contactor

Nicholas B. Wyatt, Timothy J. O'Hern, and Bion Shelden
Engineering Sciences Center, Thermal/Fluid Experimental Sciences Department, Sandia National Laboratories, Albuquerque, NM 87185

DOI 10.1002/aic.14109
Published online April 16, 2013 in Wiley Online Library (wileyonlinelibrary.com)

Annular centrifugal contactors were developed as single, compact units utilized to transfer desired species between immiscible fluid phases. Critical to understanding the mass-transfer characteristics in the annular mixing region is a clear picture of the distribution of droplet sizes of the fluids involved. To date, very little experimental data appears in the literature. We fill that void by using laser fluorescence and optical methods to directly observe and measure drop-size distributions for a silicone oil/water system in a centrifugal contactor. The shape and characteristics of the log-normal distributions, including the Sauter mean diameter and distribution means, are elucidated in terms of rotor speed and organic phase fraction. The size distribution of entrained air bubbles is also examined. The results presented here will be invaluable in validating and expanding the predictive capacity of the many models that have been developed to describe the flow within these devices.
Published 2013 American Institute of Chemical Engineers *AIChE J*, 59: 2219–2226, 2013
Keywords: annular centrifugal contactor, drop diameter, multiphase mixing

Introduction

Liquid–liquid extraction is the process by which desired dissolved chemical species are extracted from one phase by mixing and subsequently separating two immiscible fluids. One tool for carrying out liquid–liquid extraction that has found widespread use is the annular centrifugal contactor. The annular centrifugal contactor is a combination mixer and separator with a single moving part (rotor) used for transfer of desired components between immiscible fluids. Originally developed at Argonne National Laboratory for nuclear waste reprocessing,[1] centrifugal contactors have since been proposed for use in a very wide variety of applications,[2] including metals extraction,[3–5] wastewater treatment,[6] pharmaceutical processing,[7,8] enantioselective chemical separations,[9] and biodiesel synthesis.[10] Centrifugal contactors are attractive unit operations due to their compact size, high efficiencies, short residence times, and high process throughputs.

During operation of the centrifugal contactor, two immiscible fluids (an organic or oil phase and an aqueous phase) are introduced into the annular region between the contactor housing and the spinning rotor via separate ports (Figure 1). The liquids mix in the gap, entraining air from the free surface, and flow down through the mixing zone to the vane region. The vanes then direct the fluids inward to the base of the rotor. Several vane plates are available having varying numbers and shapes of vanes, each producing unique effects on the mixing and flow properties of the contactor.[11] Finally, the fluids flow up into the spinning rotor where they are centrifugally separated and flow out of their respective outlets.

Mass-transfer behavior in this device is highly dependent on the interfacial area between the two liquid phases being mixed in the annular mixing zone. The distribution of drop sizes obtained for various operating parameters of flow rates, rotor speeds, and phase ratios is critical information needed to accurately predict mass-transfer effectiveness. Recently, good progress has been made in modeling the flow in the annular mixing zone using computational fluid dynamics.[12–16] As these models are extended, predictions of the interfacial area between the immiscible phases can be made. However, there exist few experimental measurements of drop sizes and interfacial areas to validate these models and predictions. Further, experimental drop size data could also be used for the selection and calibration of breakup and coalescence models for interfacial area prediction using population balance methods.

Accurately measuring the drop sizes in a centrifugal contactor and optically distinguishing between fluid droplets and air bubbles is not trivial. The turbulent flow and entrained air bubbles make direct imaging using conventional techniques difficult. Further, the high rotor speeds at which contactors are often operated (> 3000 rpm) add to the difficulty of obtaining clear images of the multiphase flow. Recently, several studies have been published in which researchers have successfully measured the characteristics of the multiphase flow using various methods. Using a chemical method suggested by Doraiswami and Sharma,[17] Kadam et al.,[18] measured the effective interfacial area in three centrifugal contactors of varying diameter and levels of power consumption. From the measured power consumption and interfacial area, they were able to estimate Sauter mean diameters of

Correspondence concerning this article should be addressed to N. B. Wyatt at nbwyatt@sandia.gov.

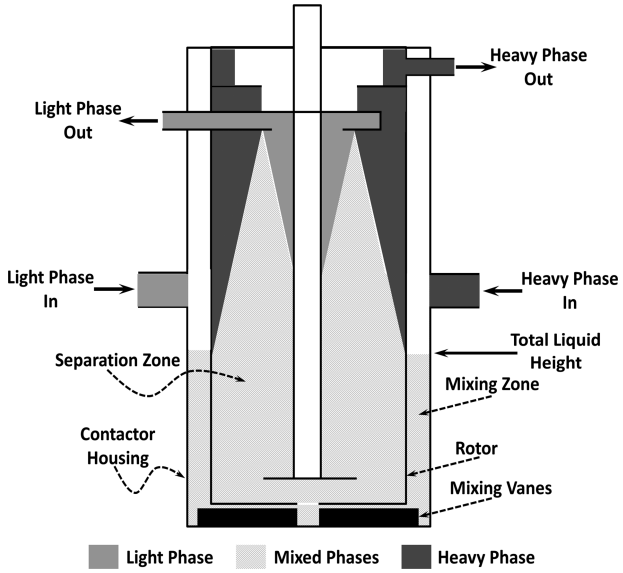

Figure 1. Simplified schematic representation of an annular centrifugal contactor.

10–50 μm for various aqueous/organic systems. However, these experiments were carried out in a liquid filled apparatus and, thus, no air was present as in the industrially used system. Later, Tamhane et al.[19] used a phase Doppler particle analyzer to measure drop sizes in the mixing zone for three different organic phases with water and report average drop sizes in the range of 30–200 μm depending on power consumption. Again, these results come from a liquid filled system which lacks air entrainment. Most recently, Schuur et al.[20] used focused beam reflectance measurements to measure drop-size distributions for very low overall flow rates (40–100 mL/min) based on measurement of reflectance which is converted to chord size distributions using a correction factor. Using this technique, they report Sauter mean diameters that range from 150 μm to over 600 μm based on varying organic flow rates for a 1,2-dichloroethane/water system.

Here we present a more direct approach at experimental drop-size distributions in an annular centrifugal contactor for conditions that more closely resemble those seen in industrial use (i.e., free surface leading to air entrainment in the mixing zone and flow rate exceeding those previously published). Using laser-based fluorescence, clear optical images of the flow are attainable that can then be analyzed to directly determine sizes and distributions of droplets in the mixing zone. We examine the effect of rotor speed on the distributions, average drop sizes, and Sauter mean diameter for a system of polydimethylsiloxane (PDMS) and water. Drop-size distributions are reported for the organic phase dispersed in an aqueous phase with a constant total (organic plus aqueous) flow rate. Further, we report measurements of air bubble size distributions from air entrained in the flow at various rotor speeds.

Materials and Methods

All of the experiments described here were performed using a CINC-V2 annular centrifugal contactor available from CINC Industries (Carson City, NV). The stainless steel contactor housing was replaced with a clear acrylic housing available from the manufacturer to enable optical measurements to be made with the contactor running. The acrylic housing was then placed in a container of refractive index matching fluid to eliminate the optical effects of surface curvature and improve image quality. The inner diameter of the housing is 2.5 in. (63.4 mm) and the rotor has a diameter of 2 in. (50.8 mm) leaving a 0.25 in. (6.35 mm) gap in the annular region. The bottom vane plate used consists of eight curved vanes having a tip-to-tip diameter of 2 3/16 in. (55.56 mm). As such, the mixing vanes extend into the annular gap, but do not extend all the way to the housing wall. The contactor was fed using two identical Masterflex L/S Easy-Load II peristaltic pumps (Model 77200-60, Cole-Parmer, Vernon Hills, IL) powered by identical Masterflex L/S variable speed motors (Model 7553-70, Cole-Parmer, Vernon Hills, IL). Tap water with no further purification was used for the aqueous phase while PDMS with a viscosity of 0.0046 Pa.s (Clearco Products, Bensalem, PA—Table 1) was used as the organic phase. For visualization, Nile red dye (Sigma-Aldrich, St. Louis, MO) was dissolved into the PDMS. The Nile red dye absorbs light in the range of 532 nm and fluoresces in the range near 600 nm.

Table 1. Properties of Interest for PDMS Used in this Study

Density	920 kg/m^3
Viscosity	0.0046 Pa.s
Surface Tension	0.0197 N/m
Interfacial Tension	0.030 N/m

Images of the flow in the contactor were obtained using a Phantom v9.1 high speed camera (Vision Research, Wayne, NJ) using a 10× magnification microscope objective (Figure 2). The lens was focused approximately 1 mm inward from the inner wall of the housing (i.e., 1 mm into the gap from the housing wall). Due to the amount of fluid in the contactor, quality, focused images could not be obtained at distances further into the annular gap. Illumination was provided by shaping a Continuum Minilite PIV Nd:YAG laser beam (Continuum, Santa Clara, CA) into a light sheet with a 5 ns pulse width. The camera was synchronized with the laser so that one laser pulse was emitted during each image acquired. The synchronization of the laser and camera provides crisp images by effectively freezing the droplet motion with the 5 ns pulse. The wavelength of this light (532 nm) causes the Nile red dye to fluoresce and become visible. A filter was placed on the camera lens to block the scattered laser light and pass only the fluorescent signal. Using this setup, we are able to visualize droplets ranging in size from 40 μm to

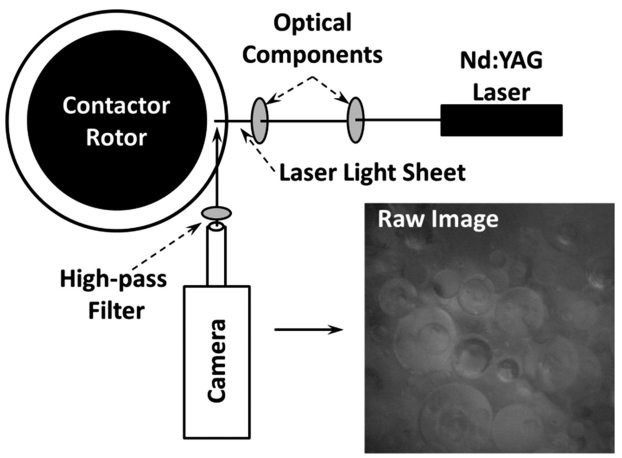

Figure 2. Schematic representation of the experimental apparatus (top view).

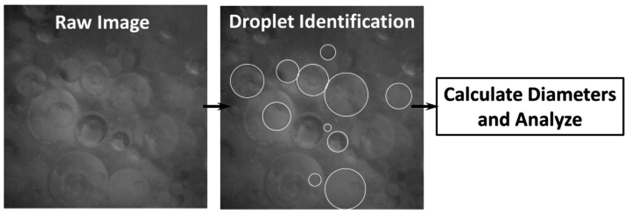

Figure 3. Schematic representation of the image analysis technique used in this study.

Some droplets were excluded in the "identification" image for clarity.

1 mm in diameter. The lower bound on the droplet size is limited by the ability to optically see droplets distinguishable by the image analysis software used here.

Images were analyzed using the public domain image processing software ImageJ (Figure 3). Droplets were fit with circles whose diameters were then calculated. All but the largest droplets were spherical in shape. The diameters of droplets that were deformed in the flow were approximated by a circle having an area equal to the distorted droplet. An image of an object of known dimensions enabled scaling to real dimensions. For each distribution, at least 1000 droplets were used in the analysis.

Results and Discussion

Effect of power consumption/rotor speed

The organic phase droplet-size distribution was measured over a range of rotor speeds spanning from 1100 to 3000 rpm (Figure 4). As reported elsewhere, the total liquid height in the mixing region varies for a given vane geometry with the rotor speed.[11,13] Also, others have reported differences in liquid hold up with varying mixing vane geometries.[11,15] As such, the total liquid height was measured as a function of rotor speed for the range of rotor speeds investigated here (Figure 5). To better compare the drop-size distributions taken at different rotor speeds, the location of each

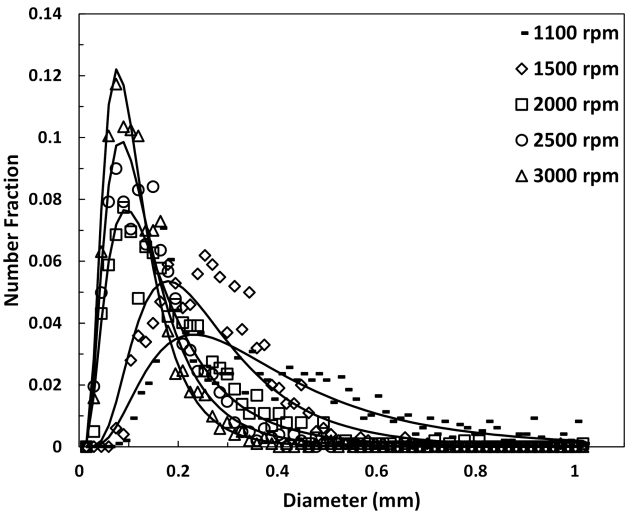

Figure 4. Organic phase droplet-size distributions for several rotor speeds.

Points indicate the experimental data while the solids lines show fits of the log-normal distribution function to the experimental data. Aqueous to organic feed ratio is 3:1 and total flow rate through the contactor is 5 mL/s.

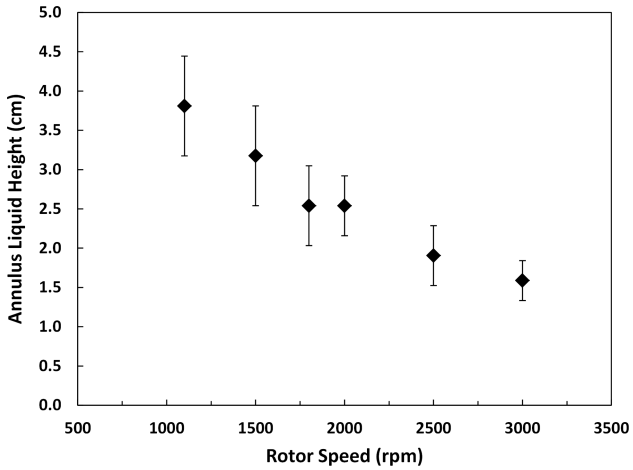

Figure 5. Effect of rotor speed on total liquid height in the mixing zone.

Error bars represent the standard deviation of at least three independent measurements. Aqueous to organic feed ratio is 3:1 and total flow rate is 5 mL/s.

measurement was adjusted to be vertically half way between the vane plate and the total liquid height. It is important to note that a different mixing vane geometry (e.g., four straight vanes) will result in different drop-size distributions as the liquid hold up and mixing will differ. Thus, the results discussed here will only apply to a system having eight curved vanes.

Often in mixing situations, the flows are described by the power number (N_p), which is a dimensionless quantity describing the ratio of resistance force to inertial force in mixing applications and is defined by

$$N_p = \frac{P}{\rho n^3 d^5} \tag{1}$$

where P is the power, ρ is the fluid density, n is the rotor rotational speed, and d is the rotor diameter. The rotor speeds examined here correspond to power number values spanning from 0.03 to 0.10 (determined from the correlation reported by Kadam et al.[18]). An estimate of the mixture density from the densities of the constituent components was used in the calculation of the power numbers here. Each droplet-size distribution was fit with a log-normal distribution function with good results. The log-normal distribution is described by

$$y(d) = \frac{1}{\delta\sqrt{2\pi}} e^{-0.5\left(\frac{\ln d - \sigma}{\delta}\right)^2} \tag{2}$$

where d is the drop diameter and δ and σ are parameters of the distribution with δ affecting the distribution height and α affecting the distribution width.[21] The log-normal shape of the distribution is consistent with what is expected for scenarios in which droplet breakup is important[22] Table 2 lists the fit parameters for the log-normal distribution for each data set shown in the present work along with a description of the dataset and the figure where it can be found. At the lowest rotor speed, the distribution of drop sizes is very broad. As the rotor speed (or power consumption) increases, the peak of the distribution shifts to lower values and the distribution narrows, meaning that the droplets in the contactor achieve a more uniform size than at low rotor speeds.

Table 2. Log-normal Distribution Fit Parameters for each Dataset Shown in this work

Phase	Rotor Speed (rpm)	Phase Ration (aq:org)	H/H_{tot}	δ	σ	Figure
Organic	1100	3:1	0.30	−1.09	0.61	4
Organic	1500	3:1	0.30	−1.43	0.54	4
Organic	2000	3:1	0.30	−1.92	0.66	4
Organic	2500	3:1	0.30	−2.12	0.60	4
Organic	3000	3:1	0.30	−2.27	0.55	4
Organic	2000	3:1	0.30	−1.92	0.66	6
Organic	2500	3:1	0.30	−2.12	0.60	6
Organic	3000	3:1	0.30	−2.27	0.55	6
Organic	2000	5:1	0.30	−1.88	0.60	6
Organic	2500	5:1	0.30	−2.10	0.61	6
Organic	3000	5:1	0.30	−2.38	0.60	6
Organic	2000	10:1	0.30	−1.80	0.63	6
Organic	2500	10:1	0.30	−2.09	0.61	6
Organic	3000	10:1	0.30	−2.48	0.63	6
Organic	1300	3:1	0.07	−1.54	0.59	8
Organic	1300	3:1	0.65	−1.14	0.63	8
Air	1300	3:1	0.07	−1.88	0.53	10
Air	1300	3:1	0.30	−0.95	0.38	10

Physically, as the rotor speed increases, the additional shear stress encountered by the fluid in the mixing zone is sufficient to break up the largest droplets in the two-phase mixture, which causes the distribution to both shift to lower droplet diameters and to become narrower around the mean.

Once the droplet-size distribution is known, the Sauter mean diameter (d_{32}) can be calculated[23] by

$$d_{32}=\frac{\sum N_i {d_i}^3}{\sum N_i {d_i}^2} \tag{3}$$

where d_{32} is the Sauter mean diameter and N_i is the number of droplets having diameter d_i. The effective interfacial area can then be estimated[24] by

$$a=\frac{6\varphi}{d_{32}} \tag{4}$$

where a is the specific interfacial area and φ is the volume fraction of the dispersed phase. The dispersed phase volume fraction was estimated from the ratio of the influent flow rates. Both the Sauter mean diameter and the mean of the distribution decrease in a power law fashion with increasing rotor speed (Figure 6). Further, the effective interfacial area increases logarithmically with increasing rotor speed. These results are both quantitatively and qualitatively similar to those reported for mixtures of 1,2-dichloroethane and water[20] and roughly one order of magnitude larger than those reported for silicone oil and glycerine.[18] The discrepancy between the results presented here and those obtained by Kadam et al. is likely due to the differences in physical properties of the aqueous phase chosen and, more importantly, the higher power consumptions studied here, which would produce smaller droplets. At high rotor speeds, the average drop diameter and Sauter mean diameter become less dependent on the rotor speed. The decrease in dependence on the rotor speed is due to a developing dynamic equilibrium between the processes of drop coalescence and drop breakup. At lower rotor speeds, the shear forces encountered in the turbulent flow act over a smaller overall interfacial area. As the large drops break up to form smaller drops, the interfacial area increases. The shear forces then have to act over a larger interfacial area. Therefore, the overall impact of rotor speed on drop size is less pronounced. The narrowing of the distribution with increasing rotor speed is again evident in the decrease in the standard deviation of the distribution, shown as error bars in Figure 6.

There are several empirical relationships in the literature that can be useful in determining mean drop size under various mixing conditions. One such relationship presented by Haas[25] for a Couette flow annular disperser (a geometry that closely resembles the centrifugal contactor) predicts the mean dispersed phase drop size as a function of the Weber number (We), the Reynolds number (Re), the viscosities of the dispersed and continuous phases (μ_d and μ_c, respectively), the gap (D), and the rotor diameter (ID).

$$\frac{d}{D}=150(We)^{-0.65}(Re)^{-0.2}\left(\frac{\mu_d}{\mu_c}\right)^{0.5}\left(\frac{D}{ID}\right)^{0.5} \tag{5}$$

The mean drop size predicted by Eq. 5 agrees qualitatively with the Sauter mean diameter reported here across the range

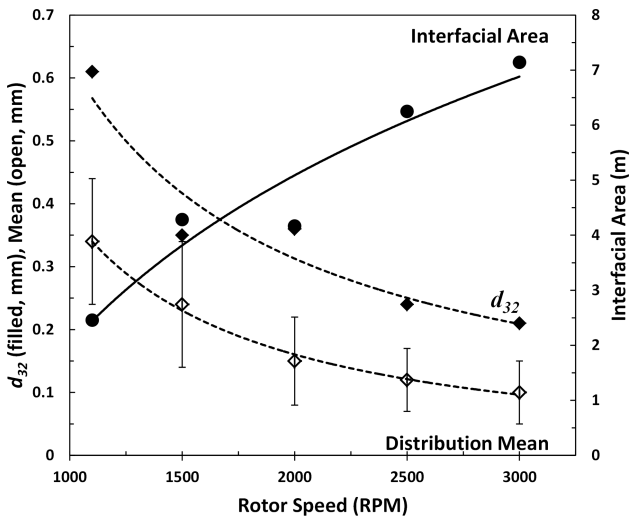

Figure 6. Effect of rotor speed on average organic phase droplet diameter, Sauter mean diameter, and interfacial area.

Lines are guides to the eye. Error bars represent the standard deviation of at least three independent measurements. Aqueous to organic feed ratio is 3:1.

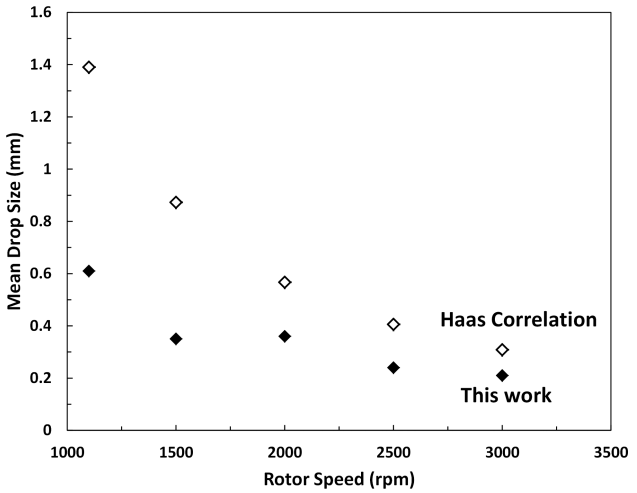

Figure 7. Comparison of Sauter mean diameter (present work) with mean drop-size prediction using Eq. 5 for the range of rotor speeds examined in this work.

of rotor speeds investigated (Figure 7) in that the trend is similar. The discrepancy between our experimental results and the prediction is greatest at the low rotor speeds (largest droplets) and decreases as rotor speed increases. This trend of high variability among predicted and experimental values for different prediction correlations was also reported by Tamhane et al.[19] The discrepancy between predicted and measured values here is likely due to the variability in dispersion apparatus and physical property differences in materials used to develop the correlations.

Effect of influent phase ratio

Next, the effect of influent phase ratio on the drop-size distribution was studied in the contactor. The feeds to the contactor are independently controlled by independent pumps allowing the examination of the effect of a wide range of flow ratios on the resulting distribution. As the fluorescent dye used in the present studies was dissolved in the organic phase, only flow ratios where the organic phase is the dispersed phase were studied (i.e., organic influent flow rate is lower than the aqueous influent flow rate). Inversion of the phases under these conditions would result in images in which droplets are not distinguishable due to the high relative concentration of fluorescent dye in each image. The drop-size distributions were measured for aqueous to organic flow ratios ranging from 3:1 to 10:1 and rotor speeds ranging from 2000 to 3000 rpm while keeping the overall flow rate into the contactor constant at 5 mL/s (Figure 8). A cursory inspection of the data shows that, in each case, the distributions are qualitatively very similar. Each distribution for each phase ratio at each rotor speed is well described by the log-normal distribution function. Further, due to the relatively high rotor speeds studied, the distributions are fairly narrow and exhibit a relatively small standard deviation. For each phase ratio studied, a weak dependence of the distribution mean on rotor speed is observed consistent with the data presented in Figure 6.

Next, the effect of influent phase ratio on the Sauter mean diameter was considered (Figure 9). Sauter mean diameter is a parameter of interest industrially in mixing and aerosol operations and is included here for completeness. For each rotor speed examined, a weak linear relationship is observed between the Sauter mean diameter and the influent phase ratio. As the organic phase fraction increases (i.e., the organic phase flow rate approaches the aqueous phase flow rate), there is little change in the Sauter mean diameter of the resulting droplets. This is consistent with the observation that the drop-size distributions exhibit a similarly weak dependence on influent phase ratio (Figure 8). The values of the Sauter mean diameter as well as the weak dependence of the Sauter mean diameter on the organic phase fraction are

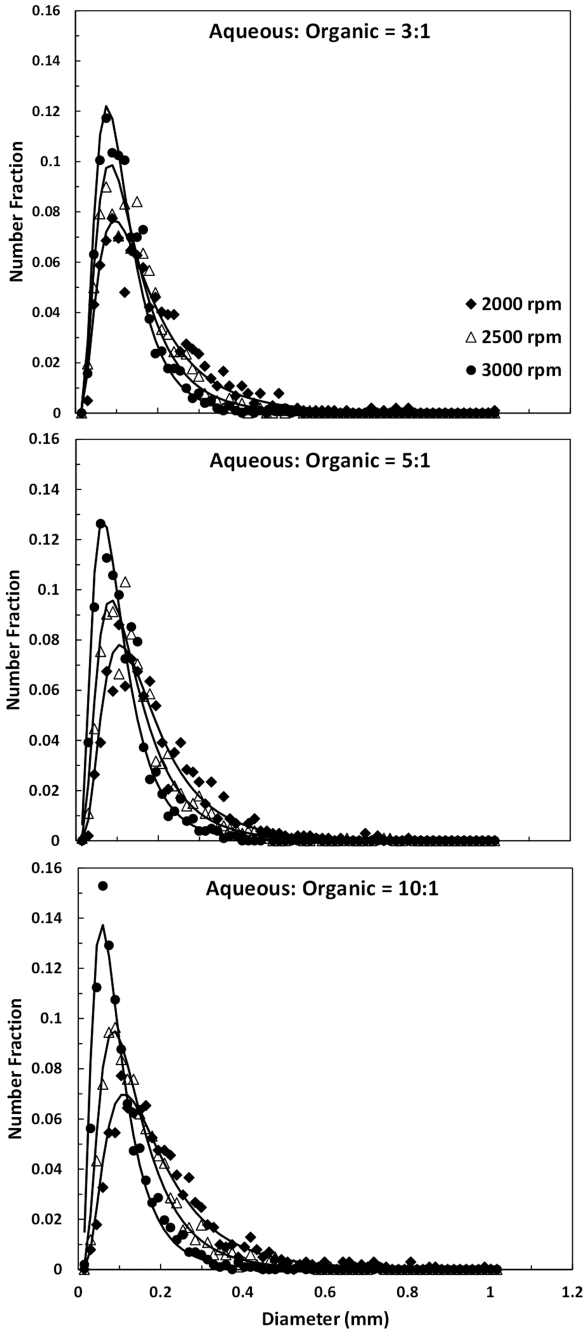

Figure 8. Effect of aqueous:organic phase ratio on the organic phase drop-size distribution for several rotor speeds for constant total flow rate of 5 mL/s.

Points represent experimental data while the lines are fits of the log-normal distribution function to the experimental data.

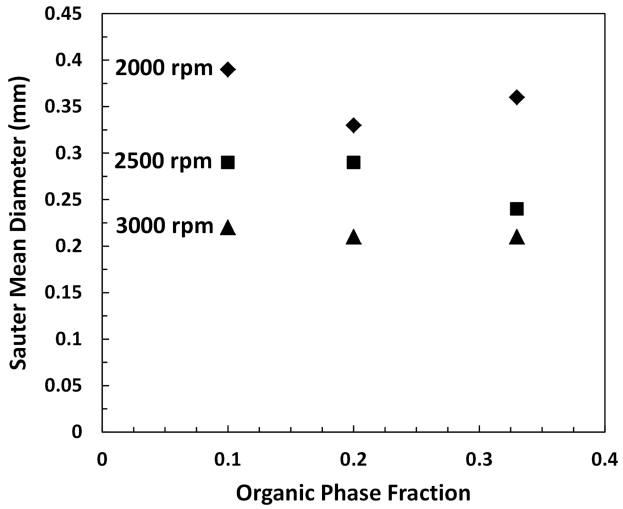

Figure 9. Effect of the organic phase fraction (organic/aqueous) on the Sauter mean diameter of the organic phase droplets for several rotor speeds.

consistent with results reported at high phase fractions by Schuur et al.[20] for a dichloroethane/water system. At lower phase ratios, Schuur et al. report a sharp increase in Sauter mean diameter and explain that this was caused by a phase inversion in the mixing zone. Such a change was not observed over the range of organic phase fractions studied here.

Spatial changes in drop-size distribution

The changes in the organic phase drop-size distribution as the mixture proceeds through the mixing zone were measured next. Measurements were taken at three vertical locations in the mixing zone corresponding to normalized heights of 0.07, 0.30, and 0.65. The total liquid height in the mixing zone varies with rotor speed and total flow rate so the locations of the measurements are reported as normalized distances based on the total liquid height. As the liquid height in the annulus oscillates in a periodic fashion,[13] the total liquid height used here refers to the distance from the bottom of the contactor to the midpoint between the maximum and minimum liquid heights measured during operation of the contactor. In all cases, the drop-size distributions are lognormal. Near the surface of the mixing zone, the drop-size distribution is very broad indicating the presence of a significant number of large droplets (Figure 10). In this location, the aqueous and organic phases are just beginning to mix and there is a significant amount of air entrainment. As the mixture proceeds down through the mixing zone, the distribution becomes much narrower as the largest droplets break up under the stresses of the turbulent flow (Figure 10).

The Sauter mean diameter, distribution mean, and effective interfacial area exhibit linear relationships with normalized height in the mixing zone (Figure 11). The Sauter mean diameter and distribution mean decrease linearly as the mixture moves from the entrance of the mixing zone to the vane region while the associated effective interfacial area increases linearly over the same distance. Here, the error bars represent the error associated with the position of the distribution peak as determined from multiple datasets at the same experimental conditions. Further, the width of the distribution (shown here by the error bars representing the standard deviation of the distribution) decreases very slightly as the mixture approaches the vane region indicating that the distribution becomes more uniform as more and more of the largest droplets are broken up under the stresses of the turbulent annular flow.

Air entrainment—air bubble size distribution

Finally, the size distribution of the entrained air bubbles in the mixing zone was measured at various vertical locations in the mixing zone. For these measurements, the contactor was run using only the organic phase without a fluorescing dye. The organic phase was chosen for air bubble measurements due to the difficulty in completely cleaning all

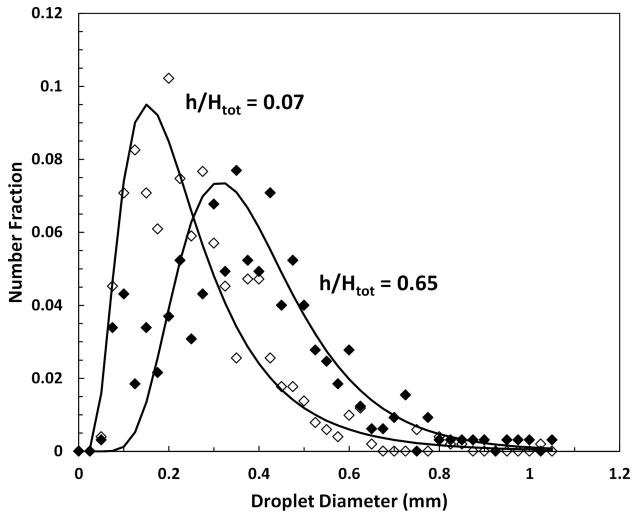

Figure 10. Organic phase drop-size distributions as a function of vertical distance in the mixing zone for a rotor speed of 1300 rpm.

For clarity, data at an intermediate vertical location was omitted from the figure. Aqueous to organic feed ratio is 3:1.

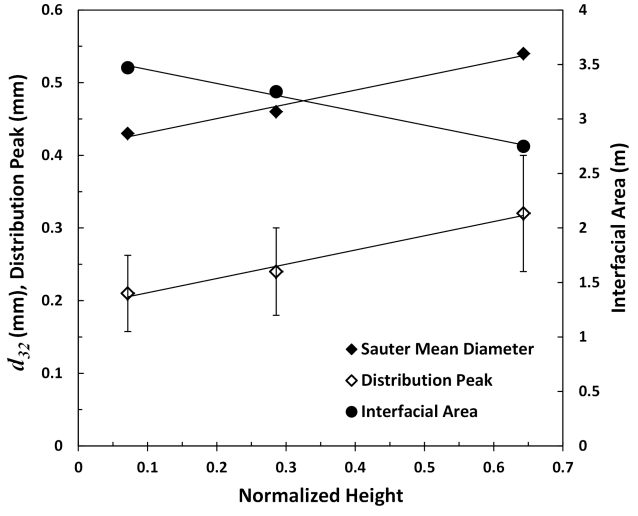

Figure 11. Average droplet diameter, Sauter mean diameter, and interfacial area as a function of the normalized vertical distance in the mixing zone for a rotor speed of 1300 rpm.

Error bars represent one standard deviation for a minimum of three independent measurements.

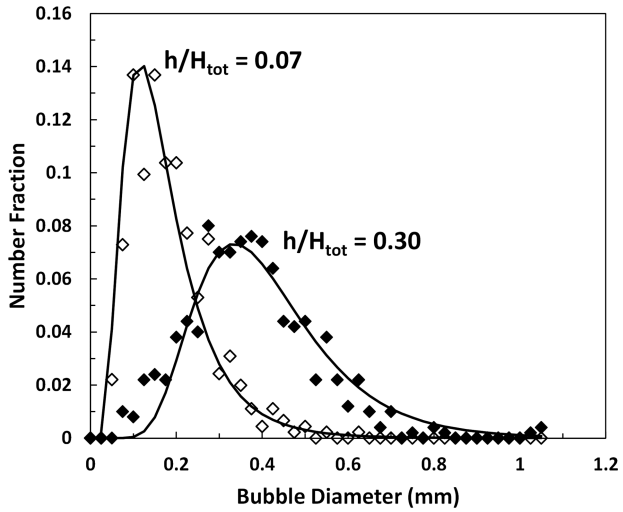

Figure 12. Size distribution of entrained air bubbles as a function of normalized vertical distance in the mixing zone for a rotor speed of 1300 rpm.

Aqueous to organic feed ratio is 3:1.

of the organic phase from the contactor and for the fact that many industrial processes use the organic phase as the continuous phase. Illumination was provided by a fiber light and the optical high-pass filter used in conjunction with the laser fluorescence studies was not used. Thus, the only bubbles/droplets visible in the resulting images were due to air bubbles that were entrained in the organic phase due to the turbulent flow and free liquid surface.

Qualitatively, the distributions of the air bubbles in the mixing zone closely resemble the droplet distributions of the organic phase when multiphase flow was studied (Figure 12). This similarity in the data may be surprising as one would expect the air bubbles to be larger than the measured liquid droplets. The observed small sizes of air bubbles reported here are likely due to the fact that our observation point is near the housing wall where the heavier organic phase is concentrated due to centrifugal motion. If the measurement could be repeated at a location closer to the rotor surface, one would likely find a different size distribution of the entrained air bubbles. In all cases reported here, the distributions are well described by the log-normal distribution function with the broadest distribution obtained near the free surface. As the mixture progresses through the mixing zone, the largest air bubbles are broken up under the stresses of the turbulent flow and the distribution shifts to smaller average values and becomes much narrower.

The average number of air bubbles observed per image captured decreases significantly from the surface of the mixing zone to the rotor zone. This observation was confirmed visually during operation of the contactor and appears to be in contradiction to observations by Wardle et al.[11] The apparent difference in observations likely stems from the fact that our measurements are taken near the inner wall of the housing rather than below the rotor and between the vanes as reported by Wardle et al. The observation of fewer bubbles near the housing wall in the vane region could be due to a large number of air bubbles migrating and escaping the flow via the free surface due to buoyancy effects. An alternative explanation is that, as the camera is focused near the inner wall of the housing, the air bubbles are not as visible because they are displaced by the heavier organic phase due to centrifugal motion.

Conclusions

Effective liquid–liquid extraction is highly dependent on the surface area between the liquids involved in the mass transfer. To this end, we have characterized the drop-size distributions obtained under various conditions of rotor speed, phase ratio, and vertical location in the mixing zone of an annular centrifugal contactor for a curved mixing vane geometry and a single total inlet flow rate. The data presented here will be significant for validation of models developed to describe both the flow and mass-transfer characteristics in centrifugal contactors, as well as increasing fundamental understanding of contactor flows.

The size distribution of both the organic phase droplets and entrained air bubbles is well described by the log-normal distribution function. For the organic phase droplets, the distribution narrows and shifts to lower droplet diameters with increasing rotor speed as the largest droplets break up under the increased shear stresses in the turbulent flow. The aqueous to organic flow phase ratio has a weak effect on the Sauter mean diameter, distribution mean, and effective interfacial area for a constant flow rate. In the mixing zone, the distribution begins as a broad log-normal distribution near the free surface and evolves to be a relatively narrow log-normal distribution in the vane region. Similar dependence on the vertical position in the mixing zone was observed for the size distribution of entrained air bubbles. To our knowledge, this is the first report of drop-size distribution data as a function of vertical distance in an annular centrifugal contactor.

Future research focusing on how the distributions change with the organic phase being continuous with the aqueous phase dispersed would be useful as this more closely matches several industrial processes. Further, the results presented here were collected using a single mixing vane geometry. Varying the geometry of the mixing vanes would change the liquid hold up and mixing behavior and, thus, have an effect on the resulting drop-size distribution. This is another area to be explored in future research endeavors.

Acknowledgments

This work was supported by the Laboratory Directed Research and Development program at Sandia National Laboratories. Sandia National Laboratories is a multiprogram laboratory managed and operated by Sandia Corporation, a wholly owned subsidiary of Lockheed Martin Corporation, for the U.S. Department of Energy's National Nuclear Security Administration under contract DE-AC04-94AL85000.

Literature Cited

1. Bernstein G, Grosvenor D, Lenc J, Levitz N. Development and performance of a high-speed annular centrifugal contactor. Technical Report ANL-7969. Argonne National Laboratory, Argonne, IL, 1973.
2. Vedantam S, Joshi JB. Annular centrifugal contactors—a review. *Chem Eng Res Des*. 2006;84:522–542.
3. Zhou X, Zhou J, Zhang C, Yu W. Application of annular centrifugal contactor on separating indium from iron. *Sep Sci Technol*. 1997;32:2705–2713.
4. Zhou J, Duan W, Zhou X, Zhang C. Application of annular centrifugal contactors in the extraction flowsheet for producing high purity yttrium. *Hydrometallurgy*. 2007;85:154–162.

5. Yarbro SL, Schrieber SB. Using process intensification in the actinide processing industry. *J Chem Technol Biotechnol.* 2003;78:254–259.
6. Xu JQ, Duan WH, Zhou XZ, Zhou JZ. Extraction of phenol in wastewater with annular centrifugal contactors. *J Hazard Mater*. 2006;131:98–102.
7. Meikrantz DH, Macaluso LL, Flim WD, Heald CJ, Mendoza G, Meikrantz SB. A new centrifugal contactor for pharmaceutical processes. *Chem Eng Commun*. 2002;189:1629–1639.
8. Zhou J, Duan W, Zhou X, Zhang C. Extraction of hydrocortisone from the fermentation liquor with annular centrifugal contactors. *Sep Sci Technol*. 2006;41:573–581.
9. Schuur B, Floure J, Hallett AJ, Winkelman JGM, de Vries JG, Heeres HJ. Continuous chiral separation of amino acid derivatives by enantioselective liquid-liquid extraction in centrifugal contactor separators. *Org Process Res Dev*. 2008;12:950–955.
10. Kraii GN, Schuur B, van Zwol F, van de Bovenkamp HH, Heeres HJ. Novel highly integrated biodiesel production technology in a centrifugal contact separator. *Chem Eng J*. 2009;154:384–389.
11. Wardle KE, Allen TR, Anderson MH, Swaney RE. Experimental study of the hydraulic operation of an annular centrifugal contactor with various mixing vane geometries. *AIChE J*. 2010;56:1960–1974.
12. Wardle KE, Allen TR, Swaney R. Computational fluid dynamics (CFD) study of the flow in an annular centrifugal contactor. *Sep Sci Technol*. 2006;41:2225–2244.
13. Wardle KE, Allen TR, Anderson MH, Swaney RE. Free surface flow in the mixing zone of an annular centrifugal contactor. *AIChE J*. 2008;54:74–85.
14. Wardle KE, Allen TR, Swaney R. CFD simulation of the separation zone of an annular centrifugal contactor. *Sep Sci Technol*. 2009;44:517–542.
15. Wardle KE, Allen TR, Anderson MH, Swaney RE, Analysis of the effect of mixing vane geometry on the flow in an annular centrifugal contactor. *AIChE J*. 2009;55:2244–2259.
16. Deshmukh SS, Vedantam S, Joshi JB. Computational flow modeling and visualization in the annular region of annular centrifugal extractor. *Ind Eng Chem Res*. 2007;46:8343–8354.
17. Doraiswami LK, Sharma MM. Heterogeneous Reaction: Analysis, Examples and Reactor Design, Vol. 2. New York: Wiley, 1984.
18. Kadam BD, Joshi JB, Koganti SB, Patil RN. Dispersed phase hold-up, effective interfacial area and Sauter mean drop diameter in annular centrifugal extractors. *Chem Eng Res Des*. 2009;87:1379–1389.
19. Tamhane TV, Joshi JB, Mudali K, Natarajan R, Patil RN. Measurement of drop size characteristics in annular centrifugal extractors using phase Doppler particle analyzer (PDPA). *Chem Eng Res Des*. 2012;90:985–997.
20. Schuur B, Gerard KN, Winkelman JGM, Heeres HJ. Hydrodynamic features of centrifugal contactor separators: experimental studies on liquid hold-up, residence time distribution, phase behavior and drop size distributions. *Chem Eng Processing: Process Intensification*. 2012;55:8–19.
21. Lovick J, Mouza AA, Paras SV, Lye GJ, Angeli P. Drop size distribution in highly concentrated liquid–liquid dispersions using a light back scattering method. *J Chem Technol Biotechnol*. 2005;80:545–552.
22. Siegel AF, Sugihara G. Moments of particle size distributions under sequential breakage with applications to species abundance. *J Appl Probab*. 1983;20:158–164.
23. Michaelides EE. Particles, Bubbles, and Drops. New Jersey: World Scientific, 2006.
24. Westerterp KR, vanSwaaij WPM, Beenackers AACM. Chemical Reactor Design and Operation. Chichester: Wiley, 1987.
25. Haas PA. Turbulent dispersion of aqueous drops in organic liquids. *AIChE J*. 1987;33:987–995.

Manuscript received Dec. 20, 2012, and revision received Mar. 11, 2013.